THE ASTROPHYSICAL JOURNAL, 493:1–9, 1998 January 20

EMISSION LINE AND ULTRAVIOLET TO X-RAY CONTINUUM CORRELATIONS: CONSTRAINTS ON THE ANISOTROPY OF THE IONIZING CONTINUUM IN ACTIVE GALACTIC NUCLEI

TING-GUI WANG, YOU-JUN LU, AND YOU-YUAN ZHOU
Center for Astrophysics, University of Science and Technology of China, Hefei, Anhui 230026, People's Republic of China; tw@cfasun.cfa.ustc.edu.cn
Received 1996 November 5; accepted 1997 September 2

ABSTRACT

Anisotropic emission of the ionizing continuum is a general prediction of accretion disk models. In this paper, we present the results of correlation analysis of the UV emission line and UV to X-ray continuum properties for a large sample of broad emission line AGNs observed with *ROSAT*, *IUE*, and *HST*. We find strong correlations between the C IV/Lyα ratio, the equivalent width of C IV, and the UV to soft X-ray spectral slope. The results are in good agreement with the photoionization calculation, suggesting that the overall ionizing continuum can well match the observed UV to soft X-ray spectrum. These results are consistent with the assumption of an isotropic ionizing continuum shape. Our analysis suggests a small range for the "big blue bump" cutoff energy for the objects in this sample, consistent with the similar results of Laor et al. and Walter & Fink based on continuum properties. The mean UV to X-ray spectral slope is similar to the soft X-ray spectral slope. This similarity also holds for radio-loud and radio-quiet objects separately. This suggests that the two might be drawn from the same distribution. The two spectral slopes are only weakly correlated. The UV to X-ray spectral index is correlated with absolute optical magnitude. This result confirms the earlier suggestion that the ionizing continua are softer for higher luminosity objects.

Subject headings: galaxies: nuclei — quasars: general

1. INTRODUCTION

It is generally accepted that the enormous energy output of active galactic nuclei is produced by the accretion of material onto putative supermassive black holes. The large angular momentum present in the interstellar medium suggests that the accreted gas is most likely to form an accretion disk, and a variety of evidence for axisymmetry supports this idea. The accretion disk can be of a geometrically thin, thick, or intermediately slim form. The spectral energy distribution (SED) and the intensity of the radiation from such disks are expected to be highly anisotropic (e.g., Cunningham 1975; Laor, Netzer, & Piran 1990; Madau 1988). This effect is particularly important in the UV to X-ray band, which comes from the innermost part of the accretion disk, where general relativistic effects are important. However, direct measurement of the anisotropy of radiation in a single object is impossible because we can only measure the radiation in a specific direction. An indirect measurement made using the very extended narrow emission line region suggests that the nuclear radiation is anisotropic (e.g., Wilson 1994). However, the anisotropy evidenced in this way is expected to originate at a much larger scale (e.g., by an obscured torus) rather than in the nuclear region.

Broad emission lines that cover a wide range of ionization levels are thought to be produced by photoionization. According to the photoionization theory, the lines from different ionization levels respond to different parts of the ionizing continuum. For example, Lyα is produced by photons with energy at ≥ 13.6 eV, C IV by photons with $E \geq 48$ eV. Therefore, the line spectrum provides a way of diagnosing the shape and intensity of the ionizing continuum. Since it is impossible to resolve the broad-line region (BLR) spatially, only the total intensities of the emission lines can be obtained. The observed line ratios and equivalent widths depend on some average shape and intensity of the ionizing continuum illuminating the BLR, which should be different from the observed one if the continuum emission is anisotropic. Therefore, a comparison between the ionizing continuum required to reproduce the broad-line spectrum and the observed continuum can constrain the role of anisotropy in the continuum emission.

For individual objects, such a comparison is very difficult to make. First, the emission line spectrum depends on the input ionizing continuum, on the physical parameters, and on the chemical abundances of line-emitting gas. Since there are no independent methods other than modeling the emission spectrum to determine the physical conditions of line-emitting gas, determination of the ionizing continuum from the emission line spectrum requires accurate measurements of emission lines of individual elements over a wide range of ionization, which is usually not possible. Second, the ionizing continuum at EUV energies is not directly observable because of interstellar absorption.

However, a statistical study of this problem is feasible. The current photoionization model can explain reasonably well the average observed strong-UV lines (Netzer 1990); hence, the average physical parameters can be inferred in a statistical sense. Furthermore, a great number of UV and soft X-ray spectra have been accumulated with *IUE*, *HST*, and *ROSAT* in the past 5 yr (e.g., Wills et al. 1995; Zheng et al. 1997; Courvoisier & Paltani 1992; Brinkmann 1994). The *ROSAT* PSPC can detect the soft X-ray spectrum down to energy levels of 0.1 keV (Trümper 1983) for low-redshift AGNs. For bright high redshift quasars at redshift $z = 4$, the *IUE* and *HST* spectra can access emitted energies of up to 40 eV in the source rest frame. These observations make it possible to measure the emitted continuum up to

energies of $E \sim 10$–40 eV. If the intrinsic absorption is not significant (i.e., no strong absorption edges are seen), then the UV to X-ray spectrum can be roughly determined.

In this paper, we present a detailed study of the correlation between the broad emission line spectrum and UV to X-ray continuum properties for a large sample of AGNs observed with *ROSAT*/PSPC and *IUE*, *HST*. The sample and techniques of data reduction are presented in § 2. We present a statistical analysis in § 3. Detail photoionization calculations are compared with the statistical results in § 4, and the main conclusions are summarized in § 5.

2. THE SAMPLE AND DATA REDUCTION

The heterogeneous sample consists of 74 AGNs, the X-ray and UV spectra of which were analyzed for various purposes (Wang, Brinkman, & Bergeron 1996a; Wang, Zhou, & Gao 1996b), together with a number of AGNs observed by *HST* (Laor et al. 1994; 1995). The *ROSAT* spectra of 39 objects in this sample were taken from Wang et al. (1996a), and three are from Brinkmann et al. (1995). The X-ray spectra for the remaining 32 objects were retrieved from the *ROSAT* archive at the Max-Planck-Institut für Extraterrestrische Physik and processed in the manner described below.

The UV spectra of 66 AGNs have been retrieved from *IUE*/ULDA (Uniform Low-Dispersion Data Archive), and were processed with *IUE*/SIPS. Average spectra have been made for those objects through multiple observations. A correction was made for Galactic reddening before any line or continuum parameters were measured. The Galactic reddening was estimated from the neutral hydrogen column value given by Dickey & Lockman (1990), with a conversion factor (Diplas & Savage 1994) of

$$E(B-V) = \frac{N_{\rm H}^G}{5.51 \times 10^{21}\ {\rm cm}^{-2}}\,, \qquad (1)$$

where $N_{\rm H}^G$ is the Galactic hydrogen column density. The values of $E(B-V)$ are listed in Table 1. The uncertainty in $N_{\rm H}^G$ is about 10^{20} cm^{-2}, corresponding to an uncertainty in $E(B-V)$ of about 0.02. This introduces an uncertainty of $\sim$20% in the UV flux at 1350 Å. Note that the line ratio C IV/Lyα is almost insensitive to the reddening correction for the sample used here. No attempt has been made to correct the intrinsic reddening, as it is rather uncertain. It is likely that the intrinsic reddening is small for our sample, since the soft X-ray fitting does not suggest significant absorption above the Galactic columns (see below) for most objects.

TABLE 1

UV Emission Line and Continuum Parameters

Object	Other Name	$E(B-V)$	I[a] Lyα	EW Lyα	I[a] C IV	EW C IV	C IV/Lyα	1350 Å vf_v[b]	$\alpha_{\rm UV}$	FWHM[c] Lyα	FWHM[c] C IV
0003+199.....	Mrk 335	0.08	11.9	99	6.21	61	0.52	14.5 ± 0.9	0.60 ± 0.02	3691	3777
0007+106.....	III Zw 2	0.11	3.33	128	2.23	74	0.67	3.75 ± 0.63	1.24 ± 0.04	4155	5120
0026+129.....	PG	0.09	1.80	58	0.59	20	0.33	3.81 ± 0.85	1.40 ± 0.14	3668	3788
0050+124.....	I Zw 1	0.10	3.61	126	0.46	17	0.13	3.52 ± 0.51	1.91 ± 0.05	3364	2571
0052+251.....	PG	0.09	5.02	106	2.72	83	0.54	4.87 ± 1.35	0.12 ± 0.14	5087	6653
0119−286.....	TON S210	0.166	3.97	85	1.48	56	0.37	4.29 ± 0.55	0.59 ± 0.04	3853	5091
0121−590.....	F 9	0.06	30.8	82	8.76	26	0.28	32.0 ± 1.9	0.46 ± 0.03	3740	4630
0124+189.....	Mrk 359	0.09	2.33	53	1.41	68	0.61	3.27 ± 0.33	0.63 ± 0.06	1951	2000
0157+001.....	Mrk 1014	0.05	1.26	42	0.49	30	0.39	2.68 ± 0.48	0.43 ± 0.07	3873	4184
0203−005.....	Mrk 1018	0.05	2.11	82	0.99	72	0.47	1.97 ± 0.42	0.73 ± 0.15	3846	4847
0205+024.....	NAB	0.07	1.68	60	0.62	18	0.37	2.82 ± 0.68	1.08 ± 0.08	2566	2708
0232−090.....	NGC 985	0.06	4.21	110	2.25	66	0.53	5.26 ± 0.47	0.76 ± 0.04	6456	6765
0236−524.....	ESO 198−G24	0.06	1.14	188	1.17	177	1.03	1.75 ± 0.52	2.31 ± 0.10	4241	6686
0405−123[d].....	PKS	0.03	2.59	88	1.42	67	0.55	3.33 ± ···	0.78 ± 0.04	2282	3027
0430+052.....	3C 120	0.21	5.18	79	4.78	91	0.92	7.40 ± 0.48	0.86 ± 0.09	3595	3809
0513−002.....	AKN 120	0.22	34.0	113	13.0	51	0.38	33.6 ± 1.1	0.91 ± 0.02	6384	5710
0637−752.....	PKS	0.19	2.49	117	0.87	53	0.35	2.63 ± 0.73	0.91 ± 0.32	2515	2569
0702+646.....	VII Zw 118	0.10	5.49	87	1.70	45	0.31	6.06 ± 1.33	0.72 ± 0.08	3157	4465
0738+497.....	Mrk 79	0.11	5.19	76	4.29	63	0.83	8.24 ± 0.65	0.34 ± 0.06	4469	5552
0743+610.....	Mrk 10	0.09	2.50	136	1.17	84	0.47	2.45 ± 0.99	1.27 ± 0.10	4694	4506
0804+761.....	PG	0.06	5.26	82	2.58	49	0.49	8.01 ± 0.66	0.44 ± 0.03	5304	4444
0844+349.....	PG	0.06	3.79	77	1.29	55	0.34	5.01 ± 0.69	1.12 ± 0.03	3466	4587
0915+165.....	Mrk 704	0.07	1.46	91	0.84	63	0.57	1.81 ± 0.43	1.88 ± 0.07	3513	3759
0921+525.....	Mrk 110	0.03	4.02	133	2.66	166	0.66	2.28 ± 0.92	1.25 ± 0.08	4585	3782
0923+129.....	Mrk 705	0.07	2.73	80	2.37	49	0.87	3.54 ± 1.14	1.25 ± 0.24	3680	4103
0953+415[d].....	PG	0.00	2.33	136	1.18	86	0.51	2.06 ± ···	0.76 ± 0.10	2636	3067
0955+326[e].....	3C 232	0.03	4.30	83	1.70	34	0.39	4.82 ± ···	1.48 ± 0.05	2187	5526
1012+008.....	PG	0.07	1.17	127	0.23	31	0.20	1.20 ± 0.42	0.50 ± 0.41	4654	5933
1028+313.....	B2	0.04	1.01	63	0.55	42	0.55	1.77 ± 0.46	0.61 ± 0.10	3661	4216
1100+772.....	3C 249.1	0.07	2.27	56	0.62	57	0.27	2.81 ± 0.61	−0.58 ± 0.10	7298	9556
1103+728.....	NGC 3516	0.07	...	...	2.82	48	...	2.35 ± 0.28	1.99 ± 0.14	2738	3391
1114+445.....	PG	0.03	0.51	61	0.15	24	0.29	1.44 ± 1.70	1.66 ± 0.36	5547	2246
1116+215[e].....	PG	0.02	6.24	112	2.40	59	0.38	5.45 ± ···	0.83 ± 0.11	4220	4495
1119+120.....	Mrk 734	0.05	2.60	76	0.78	48	0.30	2.79 ± 0.44	0.39 ± 0.12	2685	5425
1202+281.....	GQ COM	0.03	0.97	89	0.80	90	0.82	1.18 ± 0.34	0.45 ± 0.18	4497	4921
1211+143.....	PG	0.05	6.63	88	2.11	49	0.32	8.08 ± 1.01	1.23 ± 0.15	3051	3228
1216+069[e].....	PG	0.03	1.87	118	1.30	117	0.70	1.38 ± ···	0.82 ± 0.07	2506	3039
1226+023[d].....	3C 273	0.00	13.6	48	7.58	39	0.56	32.1 ± ···	0.56 ± 0.03	3101	3760
1229+204.....	TON 1542	0.04	3.66	64	1.50	48	0.41	5.34 ± 0.49	0.24 ± 0.03	3489	4904
1237−050.....	NGC 4593	0.04	...	...	1.90	93	...	2.24 ± 0.22	1.90 ± 0.03	5183	3660
1244+026.....	Q	0.03	0.50	48	0.18	27	0.36	1.18 ± .34	1.40 ± 0.13	2210	2531

TABLE 1—*Continued*

Object	Other Name	$E(B-V)$	I^a Lyα	EW Lyα	I^a C IV	EW C IV	C IV/Lyα	1350 Å $\nu f_\nu{}^b$	α_{UV}	FWHM[c] Lyα	FWHM[c] C IV
1307+085.....	PG	0.04	2.64	73	1.36	62	0.52	3.34 ± 0.95	0.62 ± 0.07	3694	8253
1309+355.....	PG	0.02	0.50	45	0.22	25	0.44	1.36 ± 1.58	1.01 ± 0.23	1723	4962
1351+640.....	PG	0.04	2.66	91	0.87	27	0.33	3.39 ± 0.11	1.27 ± 0.01	4699	3615
1351+695.....	Mrk 279	0.03	6.68	101	4.64	96	0.67	5.28 ± 0.36	1.18 ± 0.05	6190	6556
1352+183.....	PG	0.04	1.61	65	0.74	46	0.46	1.97 ± 0.35	0.45 ± 0.07	4351	3927
1411+442.....	PG	0.02	1.46	78	0.46	30	0.32	2.10 ± 0.24	1.29 ± 0.03	2373	2617
1415+253.....	NGC 5548	0.04	11.0	99	8.06	74	0.73	12.5 ± 0.9	0.77 ± 0.04	6259	6316
1415+451.....	PG	0.02	1.04	74	0.48	70	0.46	1.03 ± 0.33	−1.01 ± 0.28	3404	6768
1416−129.....	PG	0.14	3.50	195	2.04	129	0.58	1.96 ± 1.31	0.69 ± 0.12	6125	6531
1426+015.....	Mrk 1383	0.06	6.54	41	1.97	27	0.30	12.5 ± 0.9	0.32 ± 0.02	4091	5707
1440+356.....	Mrk 478	0.02	4.50	82	0.81	23	0.18	5.33 ± 0.34	0.43 ± 0.05	2705	2913
1501+106.....	Mrk 841	0.04	6.30	85	3.48	48	0.55	6.89 ± 0.58	0.70 ± 0.03	4216	4673
1512+370.....	B2	0.03	1.05	58	0.67	66	0.64	1.57 ± 0.09	0.43 ± 0.02	4858	8333
1534+580.....	Mrk 290	0.03	4.39	81	2.52	74	0.55	4.31 ± 0.54	0.69 ± 0.04	4281	4987
1538+477[e].....	PG	0.03	1.45	141	0.60	66	0.41	0.68 ± ···	1.01 ± 0.15	5875	6195
1556+274.....	E	0.08	1.94	278	1.38	286	0.71	1.20 ± 0.55	0.92 ± 0.60	3746	7152
1613+658.....	Mrk 876	0.06	3.04	81	1.85	68	0.61	4.35 ± 0.38	0.74 ± 0.03	6758	8043
1634+076[e].....	PG	0.11	3.80	63	1.06	29	0.28	5.32 ± ···	1.04 ± 0.14	3738	4924
1704+608.....	3C 351	0.05	0.76	42	0.31	24	0.40	1.92 ± 1.54	0.20 ± 0.03	3544	5363
1720+309.....	Mrk 506	0.06	3.71	102	2.33	97	0.63	3.26 ± 0.78	0.36 ± 0.06	4558	5092
1721+343.....	B2	0.06	4.17	109	3.35	148	0.80	4.26 ± 1.94	0.65 ± 0.26	4208	6678
1803+676.....	KAZ 102	0.09	3.91	129	1.89	88	0.48	3.20 ± 0.36	0.80 ± 0.11	4750	5972
1821+643[d].....	KUV, H	0.03	7.22	150	3.83	100	0.53	5.56 ± ···	1.33 ± 0.09	4038	4203
1833+326.....	3C 382.0	0.16	6.26	105	6.18	149	0.99	6.38 ± 0.47	0.94 ± 0.06	13331	14694
1845+797.....	3C 390.3	0.08	2.32	178	1.34	148	0.58	1.09 ± 0.29	1.01 ± 0.07	3793	8190
1916−587.....	ESO 141−G55	0.10	10.6	87	7.25	85	0.68	13.5 ± 1.1	0.68 ± 0.03	5238	6021
2041−109.....	Mrk 509	0.08	19.5	126	11.4	104	0.58	16.2 ± 1.5	0.88 ± 0.03	5933	5454
2130+099.....	II Zw 136	0.09	5.56	82	2.10	61	0.38	5.21 ± 1.21	1.15 ± 0.05	2727	4277
2135−147.....	PKS	0.09	1.53	133	0.95	86	0.62	1.60 ± 0.39	1.18 ± 0.14	8408	9192
2209+184.....	PG	0.10	2.29	142	1.23	96	0.54	2.91 ± 1.27	0.96 ± 0.11	7702	6595
2300+086.....	NGC 7469	0.10	12.9	100	8.43	84	1.01	15.6 ± 1.22	0.88 ± 0.03	3208	4324
2308+098.....	4C 09.72	0.08	1.19	37	0.57	37	0.48	3.02 ± 0.38	0.09 ± 0.18	4195	5328
2316−000.....	NGC 7603	0.08	1.74	177	1.32	173	0.76	1.43 ± 0.98	1.12 ± 0.17	5511	6254

[a] In units of 10^{-13} ergs cm^{-2} s^{-1}.
[b] In units of 10^{-11} erg cm^{-2} s^{-1}.
[c] In km s^{-1}.
[d] From Laor et al. 1994.
[e] From Laor et al. 1995.

The spectral indices in UV (α_{UV}) are determined by fitting a power-law function ($f_\lambda \propto \lambda^{-2+\alpha_{UV}}$) to the dereddened UV spectra over several pseudo–line free windows at 1150–1180, 1335–1365, 1450–1480, and 1760–1800 Å (in the source rest frame). The continuum flux at 1350 Å has been determined by averaging the flux over the corresponding passband, while the mean deviation is taken as uncertainty. The uncertainty given in this way is purely statistical and is at the $(N-2)^{1/2}\sigma = 2\sigma$ level (where N = width of the passband/*IUE* spectral resolution $\simeq 6$ is the number of independent data points used for taking the average). The typical 1 σ level uncertainty for UV flux at 1350 Å is about 10%–20%. The emission line fluxes are measured by fitting the line profiles with multiple Gaussians. For strong lines, such as C IV and Lyα, usually two Gaussians are used if the line profile is symmetric, three Gaussians if it is asymmetric. For the S/N ratios of the spectra used here, three Gaussians provide a good fit to the data. One Gaussian is used for fitting the weak lines, such as N V, He II, and Si IV + O IV], where the line centers have been fixed at the observed wavelength. The fitting is done locally using the IRAF package. The fitted regions are 1180–1290 and 1480–1700 Å for Lyα + N V and C IV + He II, respectively. They are subject to changes when there is contamination in the fitting region, such as from geocoronal Lyα for very low redshift AGNs or when part of fitting region is shifted out of the spectral coverage. For the four objects (3C 351, PG 1411+442, PG 1351+640, and NGC 3516) with obvious associated UV line absorptions, the absorption troughs have been modeled with single Gaussians. The emission line flux is calculated by adding up all the emission line components. Because of the low S/N ratio of these data, the FWHM of the emission line is measured from the synthetic spectrum, which is constructed by putting all the individual Gaussian components together. The FWHM measured in this way is less affected by the noise or the presence of weak blemishes. These results are given in Table 1. As compared with the results of Wang et al. (1996b), the typical uncertainty due to the measurement for C IV/Lyα is about 0.12.

We have also included eight objects observed by *HST* in our sample. Among these, 3C 232 shows obvious absorptions in C IV and N V. The line and continuum parameters are taken from Laor et al. (1994, 1995), who adopted a similar but more precise model for emission lines, having better S/N ratio data but using a different method for estimating continuum flux. These lines and continuum fluxes have also been corrected for Galactic reddening.

The *ROSAT* PSPC spectra have been reduced using the EXSAS package (Zimmermann et al. 1994). The source counts were extracted from a circular region centered on the AGN with a radius of 3.′2. The background was estimated from an annular source-free region. The spectrum was corrected for vignetting and deadtime, and regrouped to at least 20 counts per bin. The spectrum was then fitted with a

single power law with Galactic absorption $N_{ph}(E) = A \exp(-\sigma_E N_H)E^{-\Gamma}$, where σ_E is the photoelectronic absorption cross section (Morrison & McCammon 1983) and N_H is the absorption column density. For most objects in the sample, a reasonable fit can be obtained with the single power law description, and the N_H values are consistent with Galactic N_H^G values in the corresponding direction (Dickey & Lockman 1990). Only seven objects (III Zw 2, I Zw 1, PKS 0405−123, 3C 120, Mrk 79, Q1244+0240, and 3C 390.3) in the sample show excessive absorptions larger than 10^{20} cm^{-2} at greater than 2 σ significant level. The X-ray spectral index (α_X) is related to the above photon index Γ by $\alpha_X = \Gamma - 1$. The results are presented in Table 2, where all error bars are quoted at the 1 σ level. In Table 2, we also present the absolute bolometric magnitudes (M_{abs}) of the sources, taken from Veron-Cetty & Veron (1996).

3. STATISTICAL ANALYSIS

From the data in Table 1 and Table 2, the UV to X-ray spectral slope is calculated using

$$\alpha_{UVX} = -0.491 \log (f_{1\ keV}/f_{1350}) , \quad (2)$$

where $f_{1\ keV}$ and f_{1350} are flux at 1 keV and 1350 Å, respectively. As we discussed in the last section, the typical uncertainty in the flux at 1350 Å due to measurement uncertainty plus the uncertainty in the Galactic reddening correction is estimated to be 40%. The typical uncertainty in the X-ray flux at 1 keV is 10%. Therefore, a combination of these will introduce a typical uncertainty in α_{UVX} of about 0.10.

We have also calculated the spectral slope (α_{EUV}) between the UV and soft X-ray at 0.2 keV. The uncertainty for X-ray flux at 0.2 keV is considerably larger than the corresponding error at 1 keV because the 0.2 keV flux is very sensitive to the absorption correction. For example, if the N_H value varies by 10^{19} cm^{-2}, the flux at 0.2 keV will change by 10%. An uncertainty of 10^{20} cm^{-2} in the N_H means an uncertainty of 160% in the 0.2 keV flux, or an uncertainty of 0.4 in α_{EVX}.

The distributions of α_{UVX} and α_X are plotted in Figure 1. The Kolmogorov-Smirnov test (Press et al. 1992) gives a probability of $P = 4\%$. Thus, the two data sets are drawn from the same distribution. Since the uncertainty in α_X is considerably larger than the uncertainty in α_{UVX}, the Kolmogorov-Smirnov test may give a false indication because of variance introduced by different uncertainties in the data. To address this concern, we take only the objects with small uncertainties in α_X. The Kolmogorov-Smirnov test gives $D = 0.22$, $P = 0.08$ for the subsample with $\sigma(\alpha_X) < 0.5$ ($N = 69$ objects), and $D = 0.18$, $P = 0.32$ for

TABLE 2

X-RAY PARAMETERS

Object	Z	M_{abs}	N_H (10^{20} cm^{-2})	νf_ν(1 keV) (10^{-12} ergs cm^{-2} s^{-1})	α_X	Reference	α_{UVX}
0003+199.....	0.025	−21.7	3.73 ± 0.17	10.7 ± 0.2	1.96 ± 0.04	1	1.55
0007+106.....	0.090	−22.7	7.85 ± 0.52	2.78 ± 0.41	1.00 ± 0.17	1	1.55
0026+129.....	0.142	−24.0	5.41 ± 1.22	3.12 ± 0.22	1.31 ± 0.30	1	1.53
0050+124.....	0.061	−23.4	6.90 ± 0.72	5.63 ± 0.24	2.05 ± 0.12	1	1.39
0052+251.....	0.155	−24.5	3.81 ± 0.50	3.76 ± 0.15	1.27 ± 0.12	1	1.55
0119−286.....	0.117	−23.9	1.45 ± 0.25	4.58 ± 0.19	1.69 ± 0.11	2	1.48
0121−590.....	0.046	−23.0	2.84 ± 0.16	18.1 ± 0.3	1.42 ± 0.05	2	1.61
0124+189.....	0.017	−20.2	4.69 ± 0.68	5.60 ± 0.27	1.31 ± 0.15	2	1.38
0157+001.....	0.163	−23.9	2.72 ± 0.91	0.67 ± 0.07	1.85 ± 0.17	1	1.79
0203−005.....	0.043	−21.3	2.71 ± 0.75	1.29 ± 0.08	1.12 ± 0.25	2	1.58
0205+024.....	0.155	−24.2	3.46 ± 0.36	1.84 ± 0.07	2.30 ± 0.09	2	1.58
0232−090.....	0.043	−22.4	3.10 ± 1.60	17.4 ± 7.9	1.68 ± 0.40	2	1.24
0236−524.....	0.045	−22.8	3.15 ± 0.24	15.2 ± 0.3	1.37 ± 0.06	2	1.03
0405−123.....	0.574	−27.7	3.27 ± 0.63	2.94 ± 0.16	1.19 ± 0.17	2	1.52
0430+052.....	0.033	−20.8	16.6 ± 0.8	26.9 ± 9.5	1.15 ± 0.33	2	1.22
0513−002.....	0.033	−22.2	10.4 ± 0.4	14.6 ± 0.2	1.61 ± 0.06	2	1.67
0637−752.....	0.656	−27.0	11.1 ± 3.1	2.18 ± 1.82	1.45 ± 0.84	2	1.53
0702+646.....	0.079	−23.1	4.16 ± 1.04	2.85 ± 0.22	1.38 ± 0.24	2	1.65
0738+497.....	0.022	−20.9	9.30 ± 1.70	41.4 ± 8.5	1.90 ± 0.24	2	1.15
0743+610.....	0.030	−21.1	4.05 ± 0.51	5.98 ± 0.23	1.31 ± 0.12	2	1.30
0821+761.....	0.100	−23.8	3.65 ± 0.58	6.21 ± 0.29	1.58 ± 0.15	2	1.55
0844+349.....	0.064	−23.9	4.15 ± 2.71	0.32 ± 0.06	1.63 ± 0.65	1	2.08
0915+165.....	0.029	−21.4	3.5 ± 1.8	17.0 ± 7.6	1.57 ± 0.40	2	1.01
0921+525.....	0.036	−20.6	1.37 ± 0.09	17.8 ± 0.2	1.40 ± 0.04	1	1.05
0923+129.....	0.029	−21.0	3.51 ± 0.47	7.20 ± 0.26	1.27 ± 0.14	1	1.34
0953+415.....	0.239	−25.6	1.47 ± 0.36	1.53 ± 0.09	1.71 ± 0.16	1	1.55
0955+326.....	0.533	−26.7	3.34 ± 4.12	0.16 ± 0.04	1.60 ± 1.29	1	2.22
1012+008.....	0.185	−24.4	3.54 ± ···	1.28 ± ···	1.66 ± ···	1	1.48
1028+313.....	0.177	−23.1	5.92 ± ···	0.65 ± ···	1.98 ± ···	3	1.70
1100+772.....	0.313	−25.8	3.45 ± 1.69	1.74 ± 0.27	1.64 ± 0.68	1	1.59
1103+728.....	0.009	−20.5	2.73 ± 0.12	24.8 ± 0.3	1.15 ± 0.04	2	0.99
1114+445.....	0.144	−23.7	1.50 ± 1.20	0.34 ± 0.05	1.36 ± 0.49	1	1.80
1116+215.....	0.177	−25.2	1.44 ± 0.20	2.18 ± 0.06	1.68 ± 0.06	1	1.69
1119+120.....	0.049	−22.0	2.64 ± ···	2.40 ± ···	1.98 ± ···	1	1.52
1202+281.....	0.165	−24.4	1.87 ± 0.28	1.50 ± 0.05	1.28 ± 0.11	1	1.44
1211+143.....	0.085	−23.9	3.25 ± 0.60	4.93 ± 0.32	2.13 ± 0.16	1	1.60
1216+069.....	0.334	−25.9	2.03 ± 0.60	1.57 ± 0.11	1.54 ± 0.24	1	1.46
1226+023.....	0.158	−26.9	1.39 ± 0.19	34.9 ± 0.9	1.07 ± 0.08	1	1.47
1229+204.....	0.064	−22.4	1.81 ± 0.20	3.65 ± 0.10	1.64 ± 0.08	1	1.57

TABLE 2—*Continued*

Object	Z	M_{abs}	N_H (10^{20} cm^{-2})	vf_v(1 keV) (10^{-12} ergs cm^{-2} s^{-1})	α_X	Reference	α_{UVX}
1237−050.....	0.009	−19.7	2.02 ± 0.61	6.77 ± 0.42	1.08 ± 0.22	2	1.26
1244+026.....	0.048	−26.2	6.23 ± 0.51	1.26 ± 0.38	0.77 ± 0.24	1	1.48
1307+085.....	0.155	−24.6	2.21 ± 0.45	1.73 ± 0.09	1.64 ± 0.16	1	1.63
1309+355.....	0.184	−24.7	0.41 ± 0.71	0.50 ± 0.08	1.29 ± 0.37	1	1.70
1351+640.....	0.088	−24.1	2.54 ± 1.80	0.36 ± 0.06	1.53 ± 0.63	1	1.97
1351+695.....	0.031	−21.2	1.80 ± 0.5	128. ± 21.	1..15 ± 0.17	2	0.81
1352+183.....	0.152	−24.0	1.89 ± 0.55	1.51 ± 0.09	1.64 ± 0.17	1	1.55
1411+442.....	0.090	−23.7	1.10 ± 1.00	0.058 ± 0.011	1.97 ± 0.46	1	2.26
1415+253.....	0.017	−20.7	1.43 ± 0.23	24.5 ± 0.80	1.30 ± 0.10	2	1.35
1415+451.....	0.114	−23.5	0.72 ± 0.42	0.55 ± 0.06	1.62 ± 0.21	1	1.63
1416−129.....	0.129	−24.1	7.21 ± 0.31	3.92 ± 0.54	1.19 ± 0.16	1	1.34
1426+015.....	0.086	−23.4	2.80 ± 0.32	6.24 ± 0.19	1.55 ± 0.09	1	1.64
1440+356.....	0.077	−23.4	1.38 ± 0.38	3.15 ± 0.30	2.32 ± 0.20	1	1.60
1501+106.....	0.036	−22.2	2.34 ± 0.27	10.0 ± 0.3	1.56 ± 0.12	1	1.41
1512+370.....	0.371	−25.6	1.14 ± 0.56	9.82 ± 0.08	1.16 ± 0.24	1	1.10
1534+580.....	0.030	−20.7	2.07 ± 0.56	3.23 ± 0.18	1.17 ± 0.21	1	1.55
1538+477.....	0.770	−27.5	...	0.20 ± ···	1.50 ± ···	3	1.75
1556+274.....	0.090	−21.8	3.50 ± 2.10	1.90 ± 0.40	1.50 ± 0.21	2	1.33
1613+658.....	0.129	−23.5	2.17 ± 0.52	3.57 ± 0.22	1.38 ± 0.20	1	1.53
1634+706.....	1.335	−30.1	4.42 ± 1.57	0.40 ± 0.04	1.38 ± 0.46	1	2.04
1704+608.....	0.371	−26.5	2.54 ± 1.21	0.48 ± 0.05	1.30 ± 0.41	1	1.79
1720+309.....	0.043	−21.7	2.31 ± 0.97	2.38 ± 0.22	0.91 ± 0.33	2	1.56
1721+343.....	0.206	−24.0	2.9 ± 1.0	45.6 ± 11.1	1.27 ± 0.25	2	0.99
1803+676.....	0.136	−23.6	4.44 ± 1.27	1.65 ± 0.14	1.39 ± 0.31	2	0.86
1821+643.....	0.297	−27.1	3.05 ± 1.52	3.89 ± 0.36	1.17 ± 0.49	2	1.57
1833+326.....	0.059	−21.3	8.6 ± 1.7	125. ± ···	1.39 ± 0.24	3	0.86
1845+797.....	0.057	−21.6	5.90 ± 0.56	12.1 ± 0.76	0.86 ± 0.14	2	0.98
1916−587.....	0.037	−22.9	5.46 ± 0.37	14.9 ± 0.4	1.37 ± 0.07	2	1.47
2041−109.....	0.035	−23.3	3.88 ± 0.41	25.8 ± 0.8	1.58 ± 0.10	2	1.39
2130+099.....	0.063	−23.6	4.65 ± ···	0.68 ± ···	2.25 ± ···	1	1.93
2135−147.....	0.200	−24.8	3.12 ± 1.35	2.46 ± 0.27	0.82 ± 0.39	2	1.40
2209+184.....	0.070	−22.3	4.89 ± ···	9.04 ± ···	1.20 ± ···	1	1.25
2300+086.....	0.017	−21.6	5.68 ± 0.27	18.2 ± 0.3	1.38 ± 0.05	2	1.46
2308+098.....	0.432	−26.0	4.07 ± 1.30	1.06 ± 0.10	1.44 ± 0.34	1	1.71
2316−000.....	0.029	−21.5	4.25 ± 0.63	3.78 ± 0.17	1.03 ± 0.17	2	1.28

REFERENCES.—(1) Wang et al. 1996; (2) this paper; (3) Brinkmann et al. 1995.

$\sigma(\alpha_X) < 0.3$ ($N = 55$). This result suggests that the different distribution indicated by the Kolmogorov-Smirnov test for the whole sample is due to objects with large uncertainties in α_X.

For this heterogeneous sample, the mean $\langle\alpha_{UVX}\rangle = 149 \pm 0.03$ is different from $\langle\alpha_X\rangle = 1.46 \pm 0.05$, where the error here and below is the uncertainty in the mean. This relation $\langle\alpha_X\rangle \simeq \langle\alpha_{UVX}\rangle$ also holds when the sample is broken down into radio-loud objects (17 radio galaxies and radio-loud quasars), where $\langle\alpha_X\rangle = 1.38 \pm 0.14$ and $\langle\alpha_{UVX}\rangle = 1.45 \pm 0.12$, and radio quiet objects, where $\langle\alpha_X\rangle = 148 \pm 0.10$ and $\langle\alpha_{UVX}\rangle = 1.51 \pm 0.07$. A similar result for $\langle\alpha_{0X}\rangle \simeq \langle\alpha_X\rangle$ has been noted by Brunner et al. (1992), Turner, George, & Mushotzky (1993), and Laor et al. (1997). We have also checked to see whether the two spectral indices have similar medians. The medians are 1.53 for α_{UVX} and 1.39 for α_X. If the uncertainty were normally distributed, the median would not be sensitive to the uncertainty. However, the error distribution in α_X is very likely asymmetrical; therefore, the small difference in the median could be due to the larger uncertainty in α_X. Subsequent analysis confirms this. When a subsample of objects with uncertainty in α_X of less than 0.2 (41 objects) is considered, the medians for α_{UVX} and α_X are 1.50 and 1.48, respectively. These analyses suggest that α_X and α_{UVX} might be drawn from the same distribution.

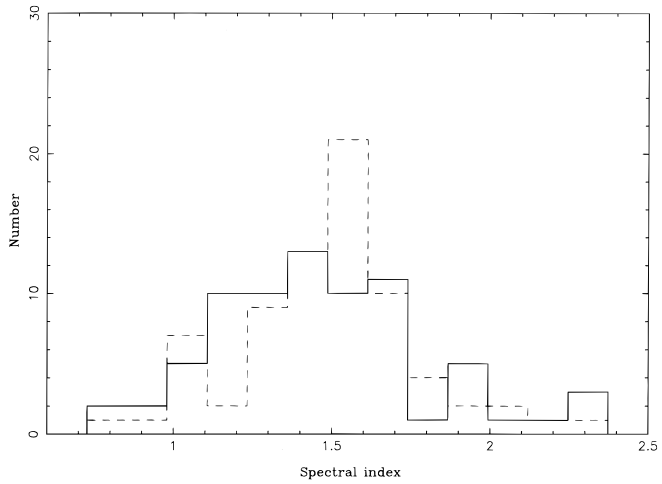

FIG. 1.—The distributions of UV to X-ray spectral slope and the soft X-ray spectral slope. Solid line represents α_X, dashed line represents α_{UVX}. Typical error bars are 0.2 for α_{UVX} and 0.5 for α_X.

Although Laor et al. (1997) claimed that the distribution of α_{0X} is bimodal, based on their sample of 23 objects and on Figure 5*b* of Wang et al. (1996b), we did not find a similar result for α_{UVX} in our sample.

Spearman rank correlation analysis has been performed among four continuum parameters: α_X, α_{UVX}, α_{UV}, and the absolute magnitude M_{abs}; and among five emission line parameters: the equivalent widths (EWs) and FWHM of

TABLE 3

CORRELATION MATRIX

		α_{SX}	α_{UVX}	α_{UV}	α_{EUV}	M_{abs}	EW Lyα	EW C IV	C IV/Lyα	FWHM Lyα	FWHM C IV
α_{SX}	R_s	1.00	0.42	−0.22	−0.09	−0.15	−0.20	−0.46	−0.43	−0.22	−0.21
	P_r	0.00	2×10^{-4}	0.06	0.46	0.22	0.09	5×10^{-5}	1×10^{-4}	0.05	0.07
α_{UVX}	R_s	0.42	1.00	−0.16	0.83	−0.50	−0.43	−0.59	−0.58	−0.28	−0.20
	P_r	2×10^{-4}	0.00	0.17	8×10^{-19}	5×10^{-6}	2×10^{-4}	3×10^{-8}	6×10^{-8}	0.02	0.08
α_{UV}	R_s	−0.22	−0.16	1.00	−0.04	0.13	0.38	0.09	−0.05	−0.09	−0.30
	P_r	0.06	0.17	0.00	0.71	0.28	1×10^{-3}	0.47	0.65	0.47	8×10^{-3}
α_{EUV}	R_s	−0.09	0.83	−0.04	1.00	−0.50	−0.30	−0.37	−0.35	−0.16	−0.10
	P_r	0.46	8×10^{-19}	0.71	0.00	5×10^{-6}	0.01	1×10^{-3}	2×10^{-3}	0.17	0.38
M_{abs}	R_s	−0.15	−0.50	0.13	−0.50	1.00	0.17	0.33	0.30	0.18	0.04
	P_r	0.22	5×10^{-6}	0.28	5×10^{-6}	0.00	0.14	4×10^{-3}	0.01	0.11	0.75
EW	R_s	−0.20	−0.43	0.38	−0.30	0.17	1.00	0.68	0.35	0.36	0.24
Lyα	P_r	0.09	2×10^{-4}	1×10^{-3}	0.01	0.14	0.00	4×10^{-11}	3×10^{-3}	2×10^{-3}	0.04
EW	R_s	−0.46	−0.59	0.09	−0.37	0.33	0.68	1.00	0.72	0.41	0.44
C IV	P_r	5×10^{-5}	3×10^{-8}	0.47	1×10^{-3}	4×10^{-3}	4×10^{-11}	0.00	3×10^{-13}	2×10^{-4}	1×10^{-4}
C IV/Lyα	R_s	−0.43	−0.58	−0.05	−0.35	0.30	0.35	0.72	1.00	0.30	0.38
	P_r	1×10^{-4}	6×10^{-8}	0.65	2×10^{-3}	1×10^{-3}	3×10^{-3}	3×10^{-13}	0.00	0.01	1×10^{-3}
FWHM	R_s	−0.23	−0.28	−0.09	−0.16	0.19	0.36	0.42	0.30	1.00	0.62
Lyα	P_r	0.05	0.02	0.47	0.17	0.11	2×10^{-3}	2×10^{-4}	0.01	0.00	5×10^{-9}
FWHM	R_s	−0.21	−0.20	−0.30	−0.10	0.04	0.24	0.44	0.38	0.62	1.00
C IV	P_r	0.07	0.08	0.08	0.38	0.75	0.04	1×10^{-4}	1×10^{-3}	5×10^{-9}	0.00

C IV and Lyα and the line ratio C IV/Lyα. This correlation matrix is presented in Table 3. Among 36 pair combinations, we found correlation caused by random factors with a probability of less than 1% for 24 pairs. Some correlations are obvious, such as between α_{UV} and α_{EUV}, and between the FWHM of C IV and the FWHM of Lyα. Some others have been discovered previously, such as the anticorrelations between M_{abs} and EW(C IV), known as the Baldwin effect, and between M_{abs} and line ratio C IV/Lyα, the positive correlations between the EWs of C IV or Lyα and the emission line width of C IV or Lyα (Wills et al. 1993), and the correlation between the line ratio C IV/Lyα and the line width of C IV or Lyα. We will not discuss these correlations, as they have been extensively discussed in the literature (e.g., Wills et al. 1993; Wang et al. 1996a).

3.1. *Correlations among Continuum Properties*

The UV to X-ray spectral slope (α_{UVX}) is correlated with absolute magnitude with a correlation coefficient $R_s = -0.50$, corresponding to a probability caused by a random factor of $P_r = 5 \times 10^{-6}$. Similarly, the α_{EUV} is correlated with M_{abs} with $R_s = -0.50$ and $P_r = 1 \times 10^{-6}$. These correlations are similar to those between α_{OX} and luminosity (e.g.,Yuan et al. 1997), indicating that the ionizing spectrum is softer when the luminosity is higher. However, neither the soft X-ray nor the UV spectral index is correlated with absolute magnitude. The α_{UVX} is weakly correlated with α_X (Fig. 2). The correlation for our heterogeneous sample is substantially weaker than that found in a sample of 58 bright Seyfert galaxies (Walter & Fink 1993). The correlation coefficient is only 0.36, corresponding to $P_r = 0.002$. Fitting the data points to a straight line (Press et al. 1992) yields $\alpha_X = (0.61 \pm 0.04) + (0.60 \pm 0.09)\alpha_{UVX}$ with a $\chi^2 = 170.5$ for 74 data points, which is accepted at a probability of only $P = 6 \times 10^{-10}$. We have taken into account both errors in the α_X (Press et al. 1992), with a typical error of 0.5 assigned for objects with no error presented in Table 2, and in the α_{UVX}, for which a typical uncertainty of 0.1 is assigned.

3.2. *Correlation between Line and Continuum Properties*

The C IV/Lyα ratio is strongly correlated with α_{UVX} with $R_s = -0.58$ (see Fig. 3), in the sense that a flat UV to X-ray spectrum corresponds to a larger C IV/Lyα. This correlation is not affected by whether or not the four objects with associated absorption lines, PG 1411+442, PG 1351+640, 3C 232, and 3C 351 (the redshift of NGC 3516 is too low to have Lyα reliably measured), are included. The UV to X-ray spectra of these four absorbed objects are very steep. We have also noted that the other AGN with $\alpha_{UVX} > 2.0$, PG 0844+349, also shows a UV C IV absorption line in the *HST* FOS spectrum (Corbin & Boroson 1996). Furthermore, radio-loud (RL) and radio-quiet (RQ) objects show no difference on the plot. This is consistent with the general indifference in the average C IV/Lyα ratio between RQ and RL QSOs (e.g., Wilkes 1986). I Zw 1, Mrk 478, and PG 1012+008 show significantly low C IV/Lyα as compared to other objects with similar α_{UVX}. Actually, their UV to X

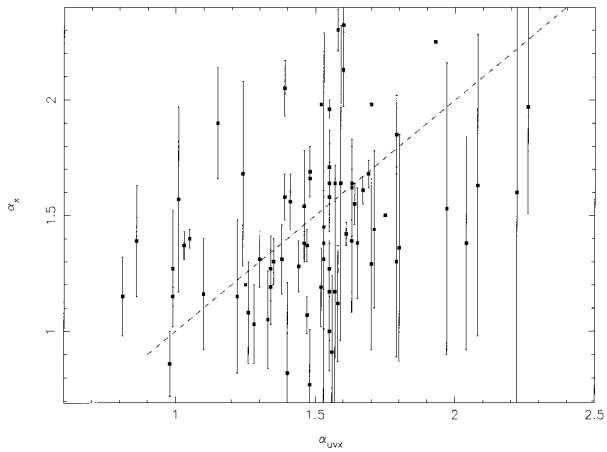

FIG. 2.—*ROSAT* PSPC spectral indices α_X versus the UV to X-ray spectral index (α_{UVX}). For data from the *ROSAT* All Sky Survey, error bars for X-ray spectral index are not shown. Dashed line represents $\alpha_X = \alpha_{UVX}$.

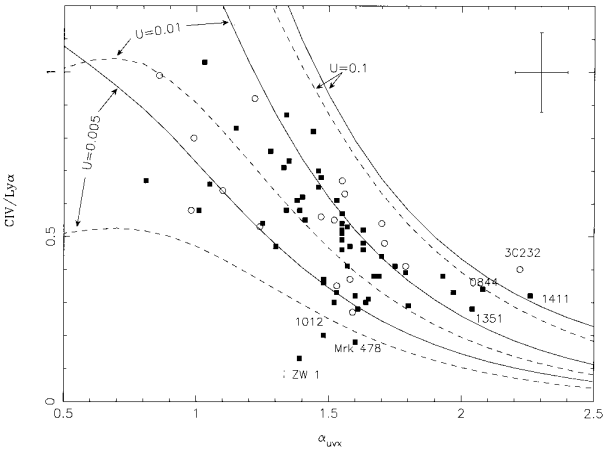

FIG. 3.—The correlation of the line ratio C IV/Lyα versus the UV to X-ray spectral index. Filled squares represent radio-quiet objects, open circles represent radio-loud objects. Theoretical predictions are shown as curves for hydrogen particle densities 10^{10} cm^{-3} (*solid line*) and 10^{9} cm^{-3} (*dashed line*). For each curve, the ionization parameters are labeled. Typical error bar is shown in the upper right corner.

spectral slopes are quite normal, while the C IV/Lyα ratios for these three are the lowest. Mrk 478 and I Zw 1 are typical narrow-line Seyfert 1 galaxies with strong optical Fe II emission (Boroson & Green 1992); it has already been noted by Wang et al. (1996b) that strong optical Fe II emitters tend to have weak C IV emission. However, the optical spectrum of PG 1012+008 is quite normal. The low C IV/Lyα ratio cannot be due to measurement error. The C IV line in the spectrum of PG 1012+008 as processed with the method of optimal extraction also appears extremely weak on the plot of Lanzetta, Turnshek, & Sandoval (1993). A correlation between the C IV/Lyα ratio and the soft X-ray spectral slope is also found, with $R_s = -0.43$, corresponding to $P_r = 4 \times 10^{-4}$.

The EW of C IV is much better correlated with α_{UVX} ($R_s = -0.59$, $P_r = 3 \times 10^{-8}$) than the Lyα EW ($R_s = -0.43$, $P_r = 2 \times 10^{-4}$; see Fig. 4). The C IV EW also appears to be correlated with α_X ($R_s = -0.46$, $P_r = 5 \times 10^{-5}$), and Lyα EW appears to be correlated with α_{UV} ($R_s = -0.38$, $P_r = 0.001$).

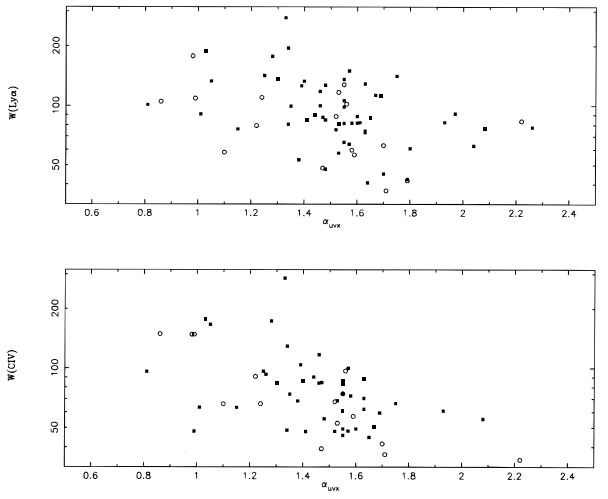

FIG. 4.—Correlations of line equivalent width with α_{UVX}. The α_{UVX} vs. EW C IV correlation is stronger than the α_{UVX} vs. EW Lyα correlation.

The correlations of line parameters with α_{EUV} are similar to those with α_{UVX} (see Table 3). The slightly lower correlation coefficients are probably due to the larger uncertainties in the 0.2 keV flux caused by the uncertainty in the absorption correction.

4. DISCUSSION

We have found strong correlations between the C IV/Lyα ratio, the C IV EW, and the observed UV to X-ray continuum shape for a large sample of AGNs observed by *ROSAT*/PSPC, *IUE*, and *HST*. These correlations have also been noted for a small sample of AGNs (Schulz 1992; Green 1996). Similar correlations between the O VI/Lyα ratio, O VI EW, and the UV to X-ray spectral slope have been reported by Zheng, Kriss, & Davidsen (1995) for a small sample of moderate-redshift AGNs observed by *IUE*, the Hopkins Ultraviolet Telescope (HUT), and *HST*. In this section, we will discuss the implications of these results.

The predicted emission line spectrum is sensitive to the exact shape of the "blue bump" in the UV to soft X-ray, since it is the photons at these energies that govern the ionization level and the excitation of the most commonly observed emission lines (e.g., Binette et al. 1989). In addition, Ferland et al. (1992) showed that the spectral shape at 0.1–1 mm can also alter the strength of the collision-excited line C IV. That the observed C IV/Lyα decreases with increasing steepness of the ionizing continuum shape in UV to X-ray is in qualitative agreement with expectations from photoionization models. One obvious suggestion is that the observed continuum shape is related to the average ionizing continuum of BLR. In the worst case, we assume that all the dispersions in the relation are due to intrinsic continuum anisotropy (see Fig. 4), and thus that the maximum anisotropy produces a scatter in $\alpha_{UVX} \simeq 1$. However, the actual situation is much better than this (see below).

In order to see how the observed data match the photoionization prediction, we have made a series of photoionization calculations using CLOUDY 84.12 (Ferland 1994). We have assumed solar abundances, because C IV is the main coolant in the ionized hydrogen (H II) zone and because C IV emission is mainly determined by the heating rate at that zone; therefore, the C IV/Lyα ratio is not very sensitive to the assumed chemical abundances (Davidson & Netzer 1979). The hydrogen column density is assumed to be 10^{23} cm^{-2}. Other values should produce similar C IV/Lyα, provided that the gas is not too optically thin. The ionization parameter (the ratio of the ionizing photon density to particle density) and particle density range from $10^{-2.5}$ to 0.1 and from 10^{9} to 10^{10} cm^{-3}, respectively. The input ionizing continuum is approximated by a power law between the far UV and 1 keV with varying spectral slope, similar to the composite EUV spectrum found by Zheng et al. (1997) for a sample of quasars observed by *HST*, but otherwise similar to the "mean AGN spectrum" of Mathews & Ferland (1987). In addition, the geometry of broad emission line cloud distribution is assumed to be spherical, so that the line intensity is the average of the emission from the illuminated and the back surfaces of the clouds. If the distribution of broad-line clouds were not a symmetrical geometry, then the line emission would be anisotropic, and the observed line ratios would depend on the inclination. For optically thick clouds, the Lyα photons are more forward beamed than C IV photons (Ferland et al. 1992). Consequently, the line ratio C IV/Lyα is larger when one looks at the illumi-

nated face, and smaller at the back face. Nevertheless, as long as some rotational symmetry is kept for the geometry and as long as there are no preferred absorptions on either the far or the near side of the clouds, the line ratios are similar for the spherical symmetric geometry (e.g., Kallman & Krolik 1986). The calculated C IV/Lyα are plotted against α_{UVX} in Figure 3.

Obviously, the observed C IV/Lyα versus α_{UVX} can be reproduced with a relatively narrow range of physical parameters. The result shows that the C IV/Lyα ratio is much more sensitive to physical conditions when the UV to X spectrum is harder. This is in good agreement with interpretations of the scatter in terms of different physical parameters. For $n_H = 10^{10}$ cm^{-3}, the range in U is about a factor of 20. This range is consistent with the results of reverberation mapping of bright AGNs for which the BLR size deviates from $R \propto L^{1/2}$ by a factor of sometimes greater than 5 (e.g., Peterson 1993; Kaspi 1997). Therefore, this interpretation is sensible. And if the typical measurement error for C IV/Lyα $\sim$ 0.12 is taken into account, the incident ionizing continuum on BLR must be very close to what we see. The UV to X-ray spectrum is likely not a power law, but a combination of "blue bump" and a hard power-law component. A different cutoff energy for the "bump" will further introduce scatter in the correlation (see below). A more detailed analysis requires higher quality data.

The correlation between the Lyα EW and the α_{UV} is a natural prediction if the observed UV spectrum extends to the Lyman limit and the BLR sees the same continuum as we do. However, the correlation between the Lyα EW and α_{UVX} requires that the continuum slope in the Lyman continuum range also be related to the α_{UVX}, since Lyα is produced mainly by recombination process. Since α_{UVX} is not correlated with α_{UV} (see § 3), the UV continuum must extend to the Lyman limit to produce the former correlation, but not to too high energy, or it would destroy the latter. The fact that α_{UV} is not correlated with C IV EW also suggests that the UV spectrum does not extend too far to the Lyα limit continuum.

For a description of the "big blue bump" as $f_\nu \propto \nu^{-\alpha_{UV}} e^{-h\nu/E_{cut}}$, it is shown that the range in the cutoff energy, E_{cut}, is small (Walter & Fink 1993; Laor et al. 1997). With this range of E_{cut}, the C IV ionizing photon numbers do not change much; however, the heating rate changes significantly if α_{UVX} is soft. As a result, the C IV/Lyα ratio is sensitive to the cutoff energy of the "big blue bump" (cf. Binette et al. 1989). Grid photoionization calculations are made for $n_H = 10^{10}$ cm^{-3}, $N_c = 10^{23}$ cm^{-2}, and solar chemical abundance, with results in agreement with the above qualitative analysis (see Fig. 5). For example, for $\alpha_{UVX} \sim 1.5$–2.0, the difference in the C IV/Lyα ratio is 0.28 if E_{cut} varies from 30 to 60 eV, similar to the value of the observed scatter in the C IV/Lyα versus α_{UVX} correlation. A larger cutoff energy range would produce a scatter larger than the one observed. This analysis provides independent evidence for a small range of cutoff energy.

Francis (1993) and Netzer, Laor, & Gondhalekhar (1992) found that the distributions of C IV and Lyα EWs are narrower than those expected for an ionizing continuum source from a randomly inclined accretion disk. Here we show that the observed α_{UVX} distribution can contribute a similar size to the scatter of Lyα and C IV EWs. Taking away the α_{UVX} factor, the distribution for Lyα EW is narrowed down significantly. If one accepts the rough isotropy of the UV to X-ray spectrum we argue for above, the random thin disk distribution of ionizing continuum strength is even more problematic.

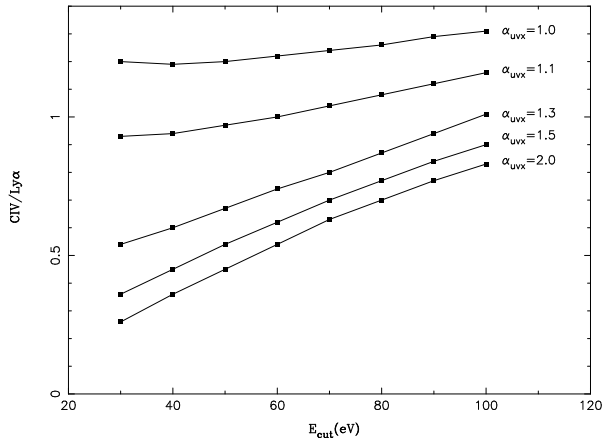

FIG. 5.—Illustration of the impact of cutoff energy of the "big blue bump" on the line ratio C IV/Lyα for various UV to X-ray spectral indices. The models adopted here use the ionization parameter $U = 0.01$, column density $N_H = 10^{23}$ cm^{-2}, and particle density $n_H = 10^{10}$ cm^{-3}.

5. CONCLUSIONS

We have presented the results of correlation analysis of UV and soft X-ray spectra for a large sample of AGN. The main results are as follows:

1. The UV to X-ray spectral indices are strongly correlated with line ratios C IV/Lyα. This correlation can be modeled with photoionization models that assume ionizing continua with a range of UV to X-ray spectral slopes, and the scatter can be interpreted as due to uncertainties in the physical conditions of the BLR. We suggest that the average ionizing spectrum striking the BLR is similar to the observed one. If the ionizing continuum consists of a power law and "big blue bump" components, the range of bump cutoff energy must be small in order to be consistent with the correlation.
2. The UV to X-ray spectral indices are significantly correlated with the EWs of C IV and Lyα. These correlations are also consistent with the intepretation of an isotropic ionizing continuum shape. As a consequence of this correlation, the constraints suggested by Netzer et al. (1992) and Francis (1993) on the anisotropy of the continuum would be even stronger.
3. The UV to X-ray spectral index is correlated with absolute optical magnitude. This result confirms earlier suggestion that the ionizing continua are softer for objects with higher luminosities.
4. The mean UV to X-ray spectral slope is similar to the soft X-ray spectral slope. This similarity also holds for radio-loud and radio-quiet objects separately. This suggests that the two may be drawn from the same distribution. The two spectral slopes are only weakly correlated.

We thank the anonymous referee for many useful suggestions that significantly improved the presentation of this paper. This work is partly supported by the Chinese Natural Science Foundation and the Panden Project.

REFERENCES

Binette, L., Prieto, A., Szuszkiewicz, E., & Zheng, W. 1989, ApJ, 343, 135
Boroson, T. A., & Green, R. F. 1992, ApJS, 80, 109
Brinkmann, W. 1994, in IAU Symp. 159, Multi-Wavelength Continuum Emission of AGN, ed. T. J. L. Courvoisier & A. Blecha (Dordrecht: Kluwer), 53
Brinkmann, W., et al. 1995, A&AS, 106, 303
Brunner, H., Friedrich, P., Zimmermann, H. U., & Stauhart R. 1992, in X-Ray Emission from Active Galactic Nuclei and the Cosmic X-Ray Background, ed. W. Brinkmann & J. Trümper (Garching: MPI), 198
Corbin, M. R., & Boroson, T. A. 1996, ApJS, 107, 69
Courvoisier, T. J.-L., & Paltani, S. 1992, *IUE*-ULDA Access Guide No. 4, (Noordwijk ESA)
Cunningham, C. T. 1975, ApJ, 202, 788
Davidson, K., & Netzer, H. 1979, Rev. Mod. Phys., 51, 715
Dickey, J. H., & Lockman, F. J. 1990, ARA&A, 28, 215
Diplas, A., & Savage, B. D. 1994, ApJ, 427, 274
Ferland, G. J. 1994, HAZY: A brief introduction to CLOUDY 84 (Lexington: Univ. Kentucky)
Ferland, G. J., Peterson, B. M., Horne, K., Welsh, W. F., & Nahar, S. N. 1992, ApJ, 387, 95
Francis, P. J. 1993, ApJ, 405, 119
Green, P. J. 1996, ApJ, 467, 61
Kallman, T., & Krolik, J. 1986, ApJ, 308, 805
Kaspi, V. M. 1997, in Emission Lines in Active Galaxies: New Methods and Techniques, ed. B. M. Peterson, F. Z. Cheng, & A. S. Wilson (San Francisco: ASP), in press
Lanzetta, K. M., Turnshek, A., & Sandoval, J. 1993, ApJ, 84, 109
Laor, A., Bahcall, J. N., Jannuzi, B.T., Schneider, D. P., & Green, R. F. 1995, ApJS, 99, 1
Laor, A., Bahcall, J. N., Jannuzi, B. J., Schneider, D. P., Green, R. F., & Hartig, G. F. 1994, ApJ, 420, 110
Laor, A., Fiore, F., Elvis, M., Wilkes, B. J., & McDowell, J. L. 1997, ApJ, 477, 93
Laor, A., Netzer, H., & Piran, T. 1990, MNRAS, 242, 560
Madau, P. 1988, ApJ, 327, 116
Mathews, W. G., & Ferland, G. J. 1987, ApJ, 323, 456
Morrison, R., McCammon, D. 1983, ApJ, 270, 119
Netzer, H. 1990, in Physics of Active Galactic Nuclei, ed. R. D. Blandford, H. Netzer, & Woltjer (Berlin: Springer), 153
Netzer, H., Laor, A., & Gondhalekhar, P. M. 1992, MNRAS, 254, 15
Peterson, B. M. 1993, PASP, 105, 247
Press, W. H., Teukolsky, S. A., Vetterling, W. T., & Flannery, B. P. 1992, Numerical Recipes in C (Cambridge: Cambridge University Press)
Schulz, H. 1992, in Physics of Active Galactic Nuclei, ed. W. J. Duschl & S. J. Wagner (Berlin: Springer), 235
Trümper, J. 1983, Adv. Space Res., 4, 241
Turner, T. J., George, I. M., & Mushotzky, R. F. 1993, ApJ, 412, 72
Veron-Cetty, M. P., & Veron, P. 1996, A Catalogue of Quasars and Active Nuclei (7th ed.; Garching: ESO)
Walter, R., & Fink, H. H. 1993, A&A, 274, 105
Wang, T., Brinkmann, W., & Bergeron, J. 1996a, A&A, 309, 81
Wang, T., Zhou, Y., & Gao, A. 1996b, ApJ, 457, 111
Wilkes, B. J. 1986, MNRAS, 218, 331
Wills, B. J., Fang, D., Steidel, C. S., & Sargent, W. L. W. 1993, ApJ, 451, 563
Wills, B. J., et al. 1995, ApJ, 447, 139
Wilson, A. S. 1994, in Proceedings of the Oxford Torus Workshop, ed. M. J. Ward (Oxford: Oxford Univ.), 55
Yuan, W., Brinkmann, W., Siebert, J., & Voges, W. 1997, A&A, in press
Zheng, W., Kriss, G. A., & Davidsen, A. F. 1995, ApJ, 440, 606
Zheng, W., Kriss, G. A., Telfer, R., Grimes, J., & Davidsen, A. 1997, ApJ, 475, 469
Zimmermann, H. U., et al. 1994, EXSAS User's Guide, MPE Report 257 (Garching: MPE)